Supporting information

Synergetic modulation on multiple transition metals enables $NiCo_xZn_yP_{(1+x+y)/2}$ microspheres for efficient lithium-ion storage

Wanying Zuo, Runhan Zhang, Yuxi Zou, Xiaoguang Fu, Zhibo Zhao, Bingqi Chen, Zibo Zhu, Hao Wang*, and Meidan Ye*

Research Institute for Biomimetics and Soft Matter, Fujian Provincial Key Lab for Soft Functional Materials Research, Department of Physics, College of Physical Science and Technology, Xiamen University, Xiamen 361005, China

*Author to whom correspondence should be addressed: h_wang@xmu.edu.cn, mdye@xmu.edu.cn

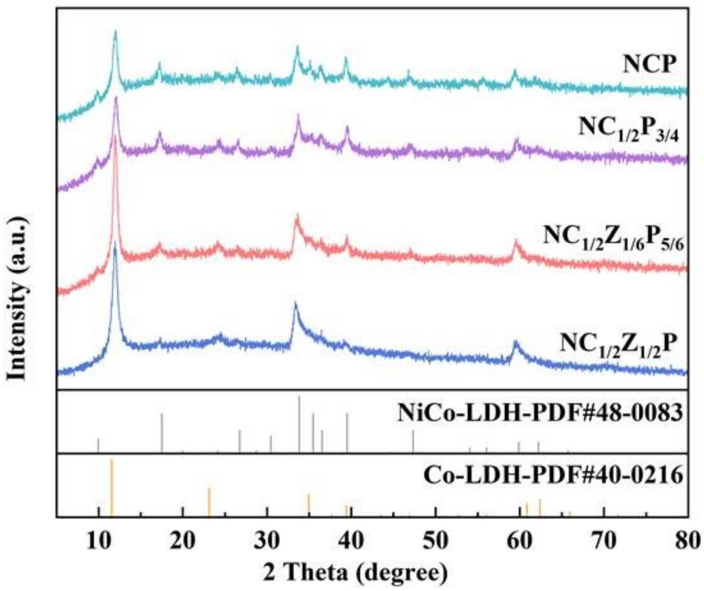

Figure S1. XRD patterns of different $NiCo_xZn_y$-LDH samples.

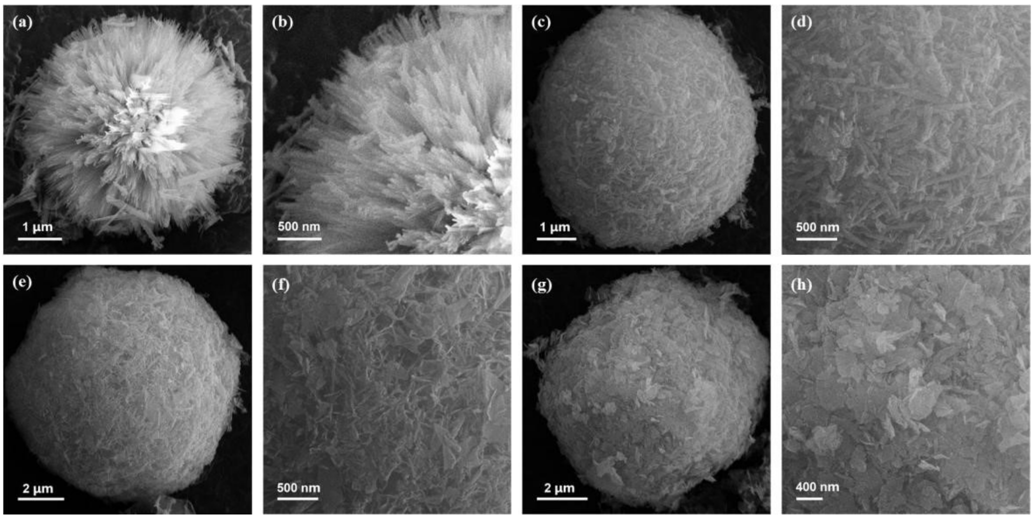

Figure S2. SEM images of (a-b) NiCo-LDH, (c-d) $NiCo_{1/2}$-LDH, (e-f) $NiCo_{1/2}Zn_{1/6}$-LDH, and (g-h) $NiCo_{1/2}Zn_{1/2}$-LDH.

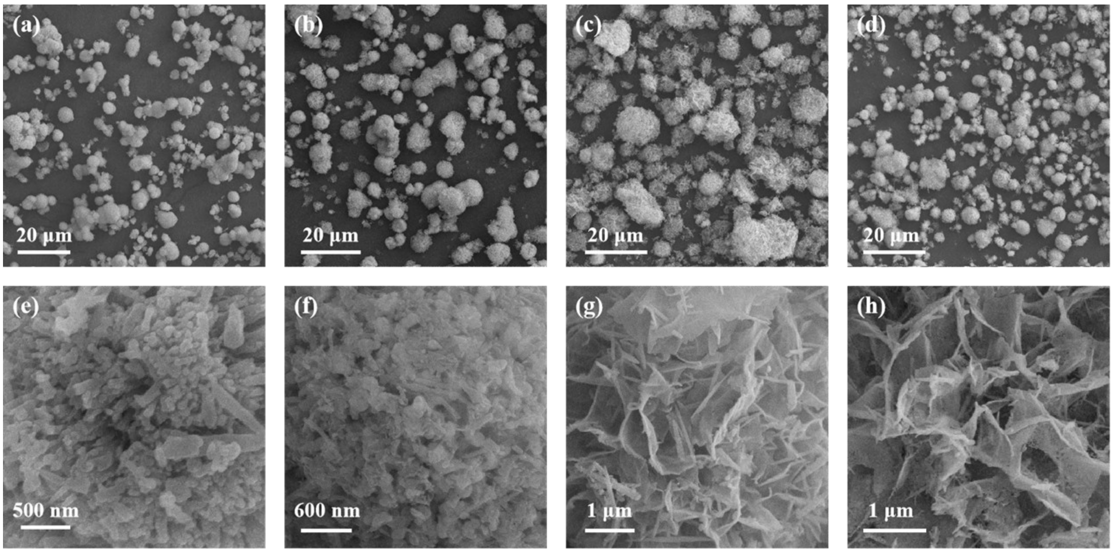

Figure S3. SEM images of (a, e) NiCoP, (b, f) $NiCo_{1/2}P_{3/4}$, (c, g) $NiCo_{1/2}Zn_{1/6}P_{5/6}$, and (d, h) $NiCo_{1/2}Zn_{1/2}P$. (a-d) Low-resolution SEM images, and (e-h) high-resolution SEM images.

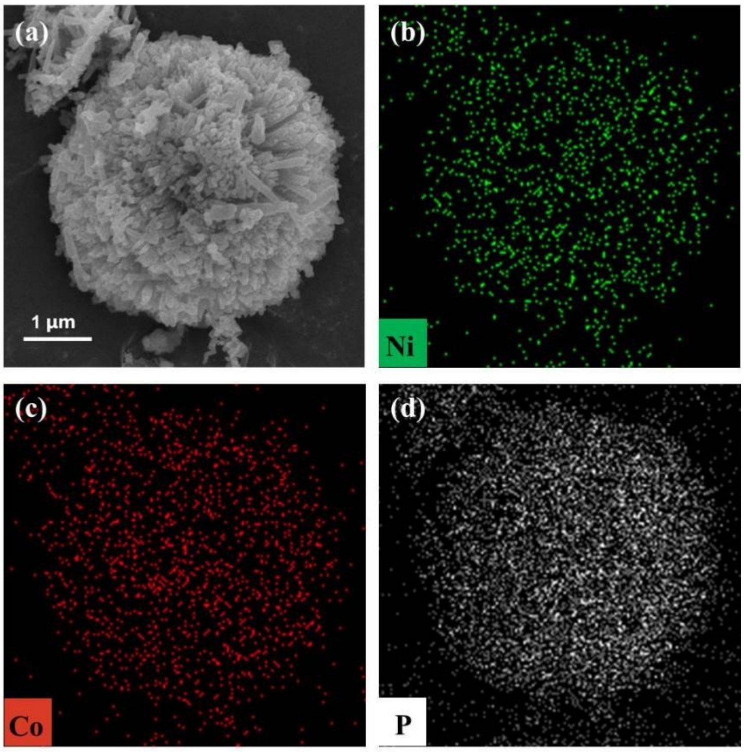

Figure S4. Elemental mappings of NiCoP.

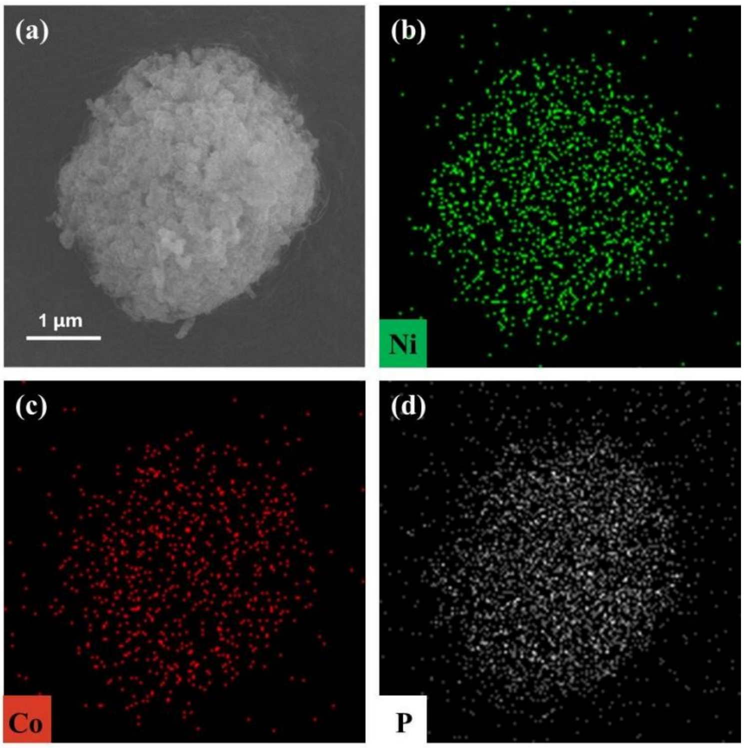

Figure S5. Elemental mappings of $NiCo_{1/2}P_{3/4}$.

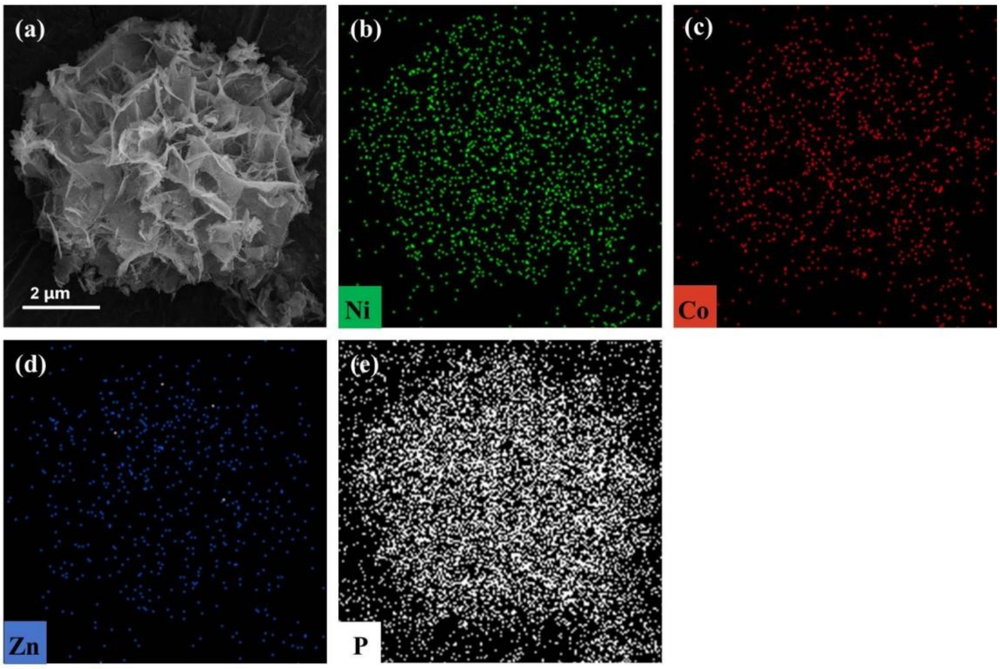

Figure S6. Elemental mappings of $NiCo_{1/2}Zn_{1/2}P$.

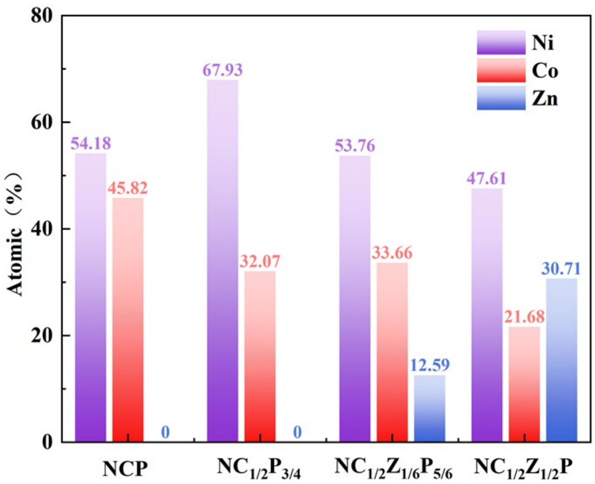

Figure S7. Metal element contents of $NiCo_xZn_yP_{(1+x+y)/2}$.

Table S1. Metal and phosphorus element contents of $NiCo_xZn_yP_{(1+x+y)/2}$.

Materials	**Atomic (%)**			
	Ni	**Co**	**Zn**	**P**
NCP	29.04	24.56	—	46.40
$NC_{1/2}P_{3/4}$	39.82	18.80	—	41.38
$NC_{1/2}Z_{1/6}P_{5/6}$	27.12	16.98	6.35	49.55
$NC_{1/2}Z_{1/2}P$	27.62	12.58	17.82	41.98

Table S2. Summary of BET results.

Materials	BET surface area (m^2 g^{-1})	Average pore diameter (nm)
NCP	31.96	10.29
$NC_{1/2}P_{3/4}$	22.15	10.53
$NC_{1/2}Z_{1/6}P_{5/6}$	37.05	11.47
$NC_{1/2}Z_{1/2}P$	42.77	11.99

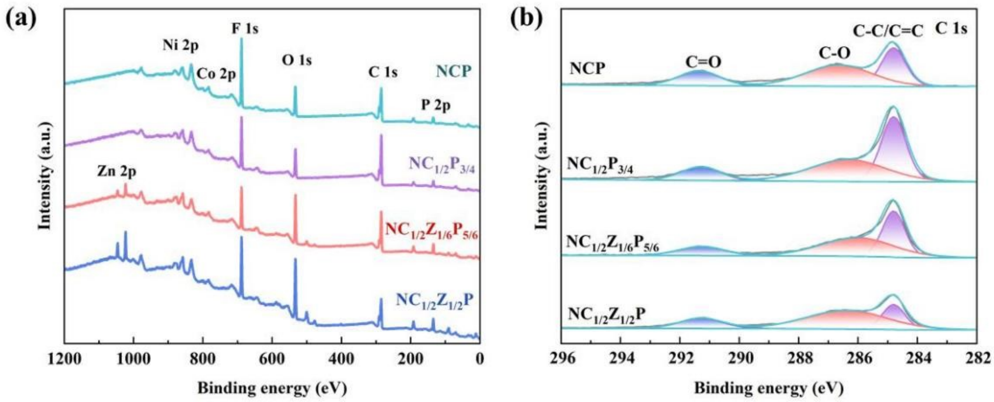

Figure S8. XPS analysis of $NiCo_xZn_yP_{(1+x+y)/2}$ ($NC_xZ_yP_{(1+x+y)/2}$) samples. (a) Full spectra, (b) high-resolution spectra of C 1s.

The calculation of D_{Li^+} values from the EIS results:

$$w = 2\pi f \qquad S(1)$$

$$Z_w = R + \sigma_w w^{-1/2} \qquad S(2)$$

where w and f are the angular frequency and frequency, σ_w is the Warburg factor that can be fitted through the slope of Z_w–$w^{-1/2}$.

$$D_{Li^+} = \frac{R^2T^2}{2A^2n^4F^4C^2\sigma_w^2} \qquad S(3)$$

D_{Li^+} is the Li^+ diffusion coefficient, A is the surface area of the electrode (1.13 cm^2), R is the gas constant, T is absolute temperature, n is the number of electrons per molecule during the reaction, F is the concentration of Li^+ and C is the Faraday constant, respectively.[1]

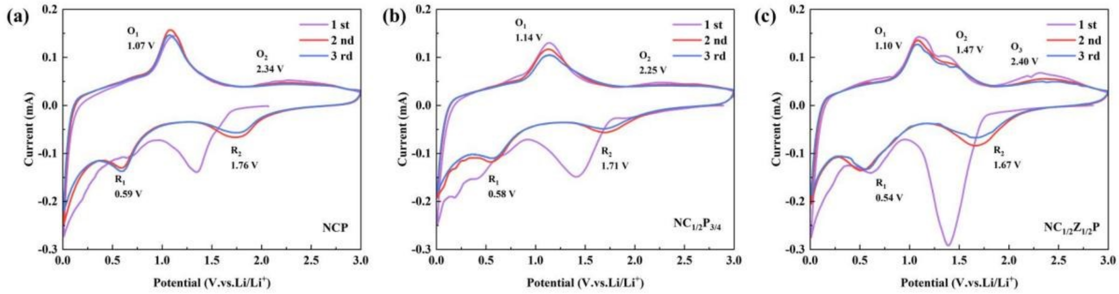

Figure S9. CV curves at 0.1 mV s^{-1}. (a) NiCoP, (b) $NiCo_{1/2}P_{3/4}$, and (c) $NiCo_{1/2}Zn_{1/2}P$.

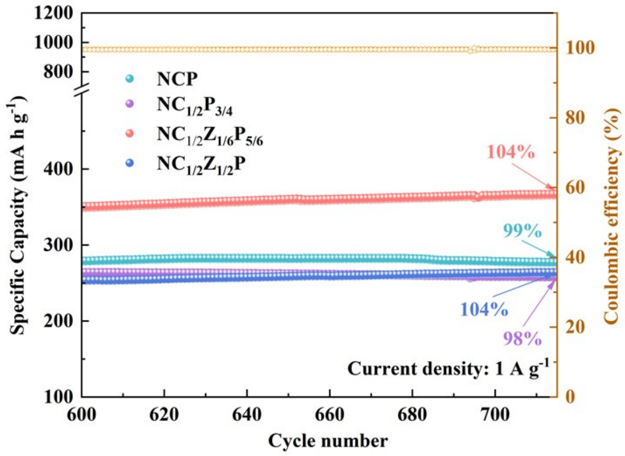

Figure S10. The cycling performance of $NiCo_xZn_yP_{(1+x+y)/2}$ ($NC_xZ_yP_{(1+x+y)/2}$) electrode-based LIBs at 1.0 A g^{-1} (details of the 600-715 cycles in **Figure 6d**).

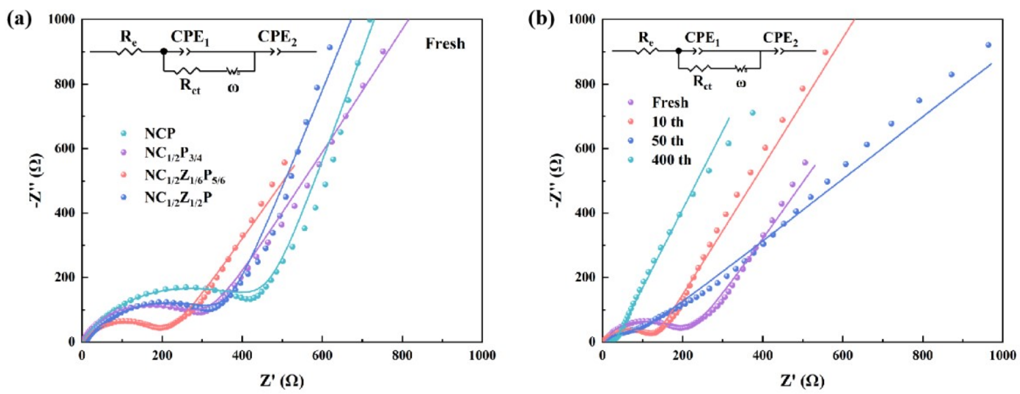

Figure S11. Electrochemical performance of $NiCo_xZn_yP_{(1+x+y)/2}$ ($NC_xZ_yP_{(1+x+y)/2}$). (a) Nyquist plots of fresh LIBs (dots: raw data; lines: fitting data), (b) Nyquist plots after different cycles (dots: raw data; lines: fitting data) of $NiCo_{1/2}Zn_{1/6}P_{5/6}$ electrode-based LIBs.

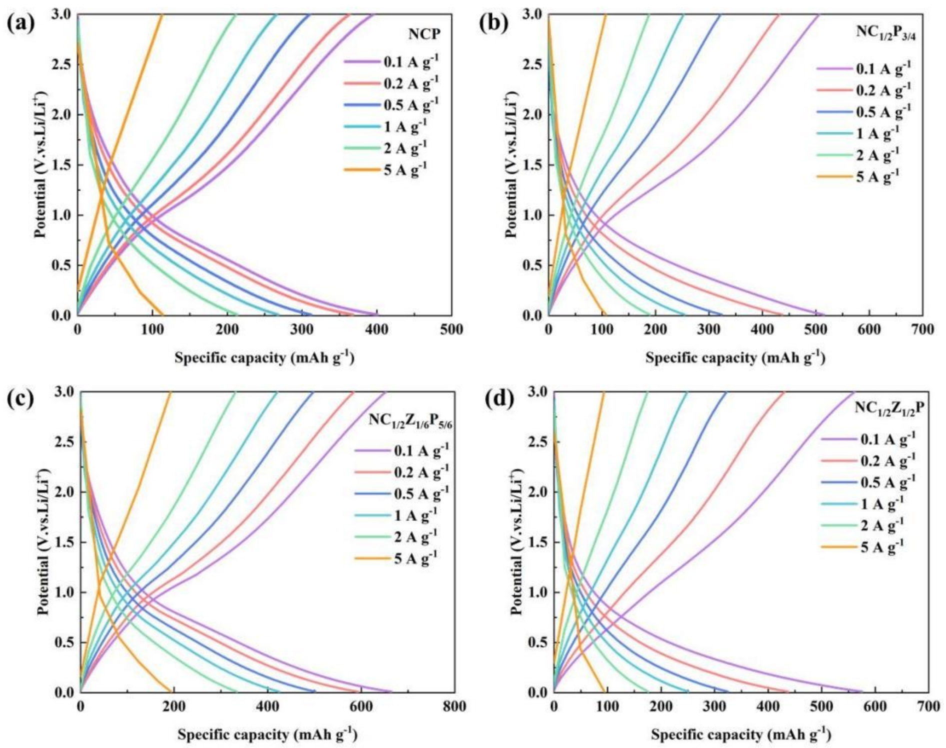

Figure S12. Charge-discharge curves at different current densities. (a) NiCoP, (b) $NiCo_{1/2}P_{3/4}$, (c) $NiCo_{1/2}Zn_{1/6}P_{5/6}$, and (d) $NiCo_{1/2}Zn_{1/2}P$.

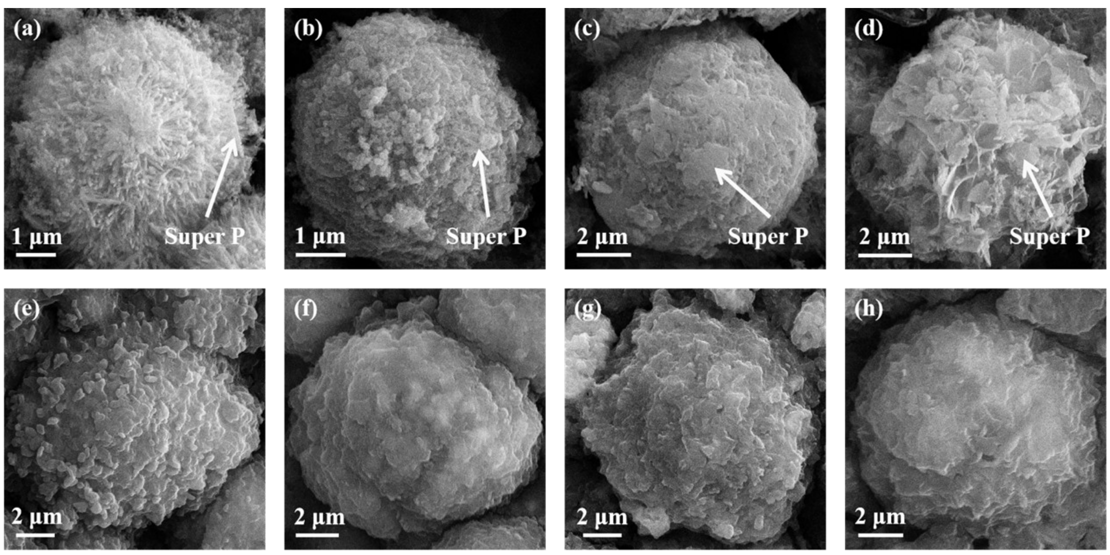

Figure S13. Ex-situ SEM images of (a,e) NiCoP, (b,f) $NiCo_{1/2}P_{3/4}$, (c,g) $NiCo_{1/2}Zn_{1/6}P_{5/6}$, and (d,h) $NiCo_{1/2}Zn_{1/2}P$. (a-d) fresh electrode plates, and (e-h) electrode plates after 400 cycles.

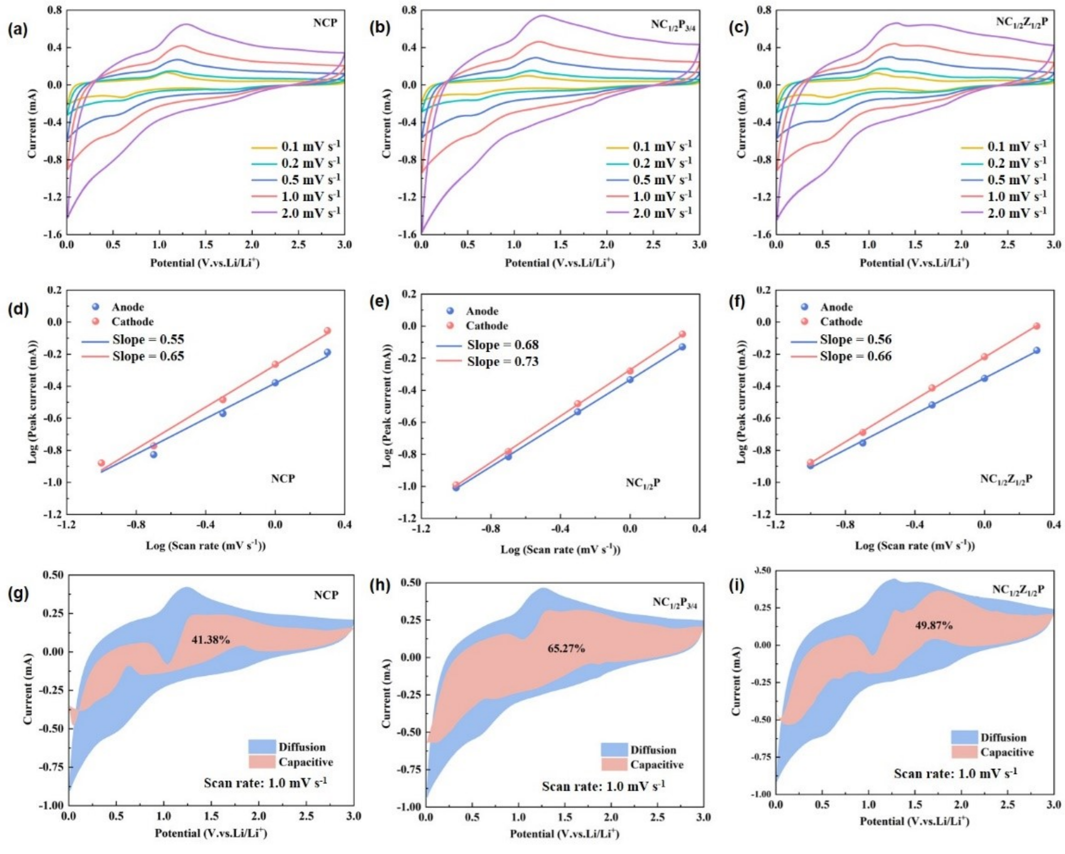

Figure S14. Electrochemical characterizations and behavior analysis of $NiCo_xZn_yP_{(1+x+y)/2}$ electrodes. (a-c) CV curves at different scan rates, (d-f) fitting plots of the peak current and scan rate, (g-i) capacitive and diffusion-controlled charge storage contributions at 1 mV s^{-1}: (a, d, g) NiCoP, (b, e, h) $NiCo_{1/2}P_{3/4}$, and (c, f, i) $NiCo_{1/2}Zn_{1/2}P$.

Table S3. LIBs performance of NiCoP electrodes reported in the literature

Material	Current density (A g^{-1})	Specific capacity (mAh g^{-1})	Cycle number	Ref.
Co_2P QDs/NPC	1.0	431.2	1600	2
CoP@C/C-0.5	0.2	638.8	500	3
Ni/Ni_2P@C-NCNTs	0.1	659.8	170	4
Co_xP@NC	1.0	526	600	5
P-NiCoP-NC-600	0.1	858.5	120	6
CoP@C⊂PCF/NCNTs	0.2	577	140	7
NiCoP	0.1	567	400	8
$Ni_{1.2}Co_{0.8}P$	1.0	260	3000	9
Ni_2P⊂pGN	0.1	514	250	10

$NiCo_{1/2}Zn_{1/6}P_{5/6}$	0.2	624	400	This work
	1.0	292	2000	
	5.0	145	10000	

References

1. S. Li, Y. Liu, X. Zhao, Q. Shen, W. Zhao, Q. Tan, N. Zhang, P. Li, L. Jiao and X. Qu, *Adv. Mater.*, 2021, **33**, 2007480.
2. X. D. Ma, C. Ji, X. Y. Yu, Y. K. Liu and X. H. Xiong, *ACS Appl. Mater. Intergaces*, 2021, **13**, 53965-53973.
3. H. Su, Y. Zhang, X. F. Liu, F. B. Fu, J. R. Ma, K. Li, W. B. Zhang, J. M. Zhang and D. Li, *J. Colloid Interface Sci.*, 2021, **582**, 969-976.
4. Y. R. Jiang, L. Zhao, H. N. Guo, C. H. An, M. Y. Yue, C. Liu and Y. J. Wang, *J. Energy Storage*, 2023, **64**, 107146.
5. Y. Liu, X. Que, X. Wu, Q. Yuan, H. Wang, J. Wu, Y. Gui and W. Gan, *Mater. Today Chem.*, 2020, **17**, 100284.
6. G. R. Ou, M. Y. Huang, X. M. Lu, I. Manke, C. Yang, J. Qian, X. M. Lin and R. J. Chen, *Small*, 2024, **20**, 2307615.
7. K. K. Guo, B. J. Xi, R. C. Wei, H. B. Li, J. K. Feng and S. L. Xiong, *Adv. Energy Mater.*, 2020, **10**, 1902913.
8. F. F. Li, J. F. Gao, Z. H. He and L. B. Kong, *J. Colloid Interface Sci.*, 2021, **598**, 283-301.
9. F. F. Li, J. F. Gao, Z. H. He, N. Brandon, X. H. Li and L. B. Kong, *Energy Storage Mater.*, 2022, **48**, 20-34.
10. C. Wu, P. Kopold, P. A. van Aken, J. Maier and Y. Yu, *Adv. Mater.*, 2017, **29**, 1604015.